

## Characterization of NiFe<sub>2</sub>O<sub>4</sub>/Ce<sub>0.9</sub>Gd<sub>0.1</sub>O<sub>1.95</sub> composite as an oxygen carrier material for chemical looping hydrogen production

Jong Ha Hwang<sup>a</sup> and Ki-Tae Lee<sup>b,c,\*</sup>

<sup>a</sup>Department of Mineral Resources & Energy Engineering, Jeonbuk National University, Jeonbuk, 54896 Republic of Korea

<sup>b</sup>Division of Advanced Materials Engineering, Jeonbuk National University, Jeonbuk, 54896 Republic of Korea

<sup>c</sup>Hydrogen and Fuel Cell Research Center, Jeonbuk National University, Jeonbuk, 54896 Republic of Korea

We investigated NiFe<sub>2</sub>O<sub>4</sub>/Ce<sub>0.9</sub>Gd<sub>0.1</sub>O<sub>1.95</sub> (GDC) composites as oxygen carrier materials for chemical looping hydrogen production (CLHP). CLHP is a promising technology to simultaneously capture carbon dioxide and produce hydrogen from fossil fuels. We found that increasing GDC content increased the amount of the hydrogen production of NiFe<sub>2</sub>O<sub>4</sub>/GDC composites. Moreover, the oxygen transfer rate for the re-dox reaction increased significantly with increasing GDC content. GDC may affect the reaction kinetics of NiFe<sub>2</sub>O<sub>4</sub>/GDC composites. The finely dispersed GDC particles on the surface of NiFe<sub>2</sub>O<sub>4</sub> can increase the surface adsorption of reaction gases due to the oxygen vacancies on the surface of GDC, and enlarge the active sites by suppressing the grain growth of NiFe<sub>2</sub>O<sub>4</sub>. The NiFe<sub>2</sub>O<sub>4</sub>/15wt% GDC composite showed no significant degradation in the oxygen transfer capacity and reaction rate during several re-dox cycles. The calculated amount of hydrogen production for the NiFe<sub>2</sub>O<sub>4</sub>/15wt% GDC composite would be 2,702 L/day per unit mass (kg).

**Keywords:** Chemical looping hydrogen production, oxygen carrier material, re-dox reaction, oxygen transfer capacity, oxygen transfer rate.

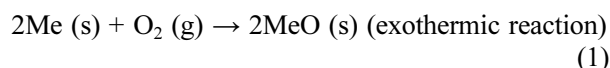
### Introduction

With the depletion of petroleum resources and the global warming phenomenon, interest in developing alternative energy sources is increasing. Hydrogen is known as a clean energy source because it emits only water during combustion and has high energy density [1-4]. Therefore, the development of efficient hydrogen production technology is becoming increasingly popular. As the use of fossil fuels increases, the emission of carbon dioxide is also increasing. Carbon dioxide contributes significantly to the greenhouse effect [5]. Therefore, various carbon capture and storage (CCS) technologies have been developed to reduce carbon dioxide emissions [6-8].

Chemical looping hydrogen production (CLHP) is a technology capable of capturing carbon dioxide at a concentration of 99% or more and simultaneously producing hydrogen at a concentration of 99% or more from fossil fuels [9-13]. While other hydrogen production technologies, such as the reforming of hydrocarbon fuel, requires the membrane separation process to obtain pure hydrogen from syngas, CLHP does not require a hydrogen separator, a pressure swing adsorption (PSA), or a carbon dioxide capture device, resulting in high

efficiency.

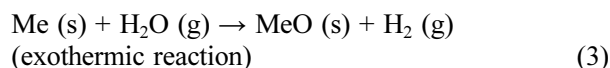
A CLHP system consists of an air reactor, fuel reactor, and steam reactor, as shown in Fig. 1. In the air reactor, the metal (Me) reacts with oxygen in the air to become metal oxide (MeO).



In the fuel reactor, the fuel such as CH<sub>4</sub> reacts with the metal oxide (MeO). The metal oxide is reduced to metal (Me) and the fuel is burned to discharge carbon dioxide and water.



In the steam reactor, the metal (Me) reacts with water to form metal oxide (MeO) and generate hydrogen.



In the above reactions, the metal oxide undergoing the re-dox reaction is called an oxygen carrier material. The transition metal oxide is usually used as an oxygen carrier material for CLHP. In the CLHP process, the oxygen carrier material plays an important role not only in transferring the oxygen required for combustion, but also in splitting water to produce hydrogen. Therefore, it is very important to develop high-performance oxygen

\*Corresponding author:  
Tel : +82-63-270-2290  
Fax: +82-63-270-2386  
E-mail: ktle71@jbnu.ac.kr

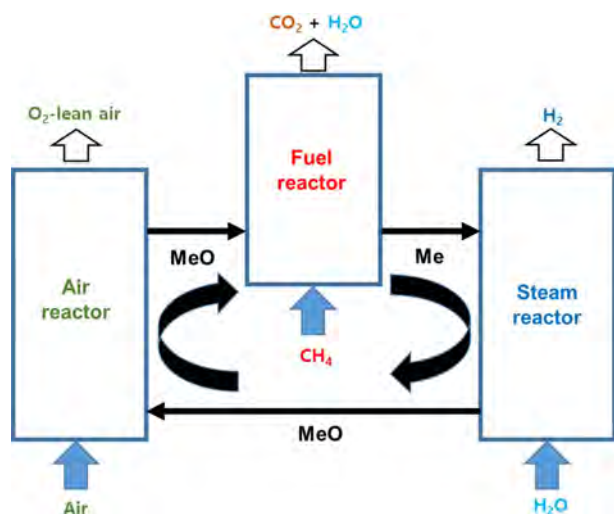


Fig. 1. Schematic of CLHP system.

carrier materials with high oxygen transfer rates, high oxygen transfer capacities, and excellent catalytic activity for water splitting. Oxides of Cu, Ni, Mn, and Sn have been used as oxygen carrier materials in CLHP. Among these metal oxides, Fe-based oxygen carrier materials have the advantages of high oxygen transfer capacity, low carbon deposition, lack of environmental harm, and low cost [14-16]. However, a conventional Fe-based oxygen carrier material such as  $\text{Fe}_2\text{O}_3$  experiences grain growth with re-dox cycling, leading to a decrease in the surface area and consequent reduction of conversion efficiency [17]. It has been reported that the  $\text{NiFe}_2\text{O}_4$  spinel phase at high temperatures exhibited higher oxygen transfer capacity and stability than individual  $\text{Fe}_2\text{O}_3$  [18, 19]. Although  $\text{NiFe}_2\text{O}_4$  exhibits oxygen carrying stability with a high oxygen transfer capacity during re-dox cycling, it still has slow re-dox reaction kinetics compared to conventional oxygen carrier materials.

To improve the re-dox reaction kinetics of  $\text{NiFe}_2\text{O}_4$ , in the present work we added gadolinium-doped ceria (GDC,  $\text{Ce}_{0.9}\text{Gd}_{0.1}\text{O}_{1.95}$ ) as a promoter to improve the oxygen transfer rate. It is well known that GDC has oxygen storage capability due to its formation of oxygen vacancies, and GDC has thus been widely used as a catalyst [20, 21]. Therefore, the addition of GDC may enlarge the reaction site. The present report describes our systematic investigation of the effects of GDC as a promoter upon the oxygen transfer properties of  $\text{NiFe}_2\text{O}_4/\text{GDC}$  composite oxygen carrier materials for CLHP.

## Experimental Procedure

$\text{NiFe}_2\text{O}_4$  powder was synthesized by a solid-state reaction method. Stoichiometric amounts of NiO (Alfa Aesar, UK) and  $\text{Fe}_2\text{O}_3$  (Alfa Aesar, UK) were mixed by ball milling in ethanol for 48 h, followed by calcination in air at  $1,200\text{ }^\circ\text{C}$  for 3 h. To make  $\text{NiFe}_2\text{O}_4/\text{GDC}$

composite oxygen carrier materials, the calculated amount of commercial GDC ( $\text{Ce}_{0.9}\text{Gd}_{0.1}\text{O}_{1.95}$ , Kceracell Co. Ltd., Korea) powder was mixed with the synthesized  $\text{NiFe}_2\text{O}_4$  powder by a ball milling process.  $\text{NiFe}_2\text{O}_4/\text{GDC}$  composite powders with various amounts of GDC (0, 5, 10, 15 wt %) were prepared by ball milling with zirconia balls for 24 h in ethanol, and the resulting mixtures were dried at  $150\text{ }^\circ\text{C}$  for 12 h.

Phase analysis was carried out by means of X-ray diffraction analysis (XRD; MAX-2500, Rigaku, Japan) using a  $\text{Cu K}\alpha$  radiation source. Diffraction patterns were recorded at the scan rate of  $4^\circ/\text{min}$  in the  $2\theta$  range of  $20^\circ$  to  $80^\circ$ . The composition of the reduced sample was confirmed by X-ray fluorescence spectrometer (XRF; PW2404, Philips, USA). The valence state of Fe in the sample was analyzed by X-ray photoelectron spectroscopy (XPS; AXIS Ultra DLD Kratos, UK) with monochromatic  $\text{Al K}\alpha$ . The morphological changes during the re-dox cycle were monitored using a field emission scanning electron microscope (FE-SEM; SN-300, Hitachi, Japan).

Temperature programmed reduction (TPR) and temperature programmed oxidation (TPO) were carried out with gas chromatography (GC; YL6100GC, Youngin, Korea) to analyze the reduction and oxidation of  $\text{NiFe}_2\text{O}_4/\text{GDC}$  composite oxygen carrier materials depending on the temperature. The temperature was increased from room temperature to  $900\text{ }^\circ\text{C}$  at a heating rate of  $3\text{ }^\circ\text{C}/\text{min}$ . 5%  $\text{H}_2/\text{Ar}$  and 10%  $\text{H}_2\text{O}/\text{Ar}$  were used as the reducing and oxidizing gases, respectively. The re-dox cycling tests were also carried out with GC. The temperature was raised to  $900\text{ }^\circ\text{C}$  at  $10\text{ }^\circ\text{C}/\text{min}$  in an Ar atmosphere and maintained for 12 h. When the temperature reached  $900\text{ }^\circ\text{C}$ , 5%  $\text{H}_2/\text{Ar}$  for reduction and 10%  $\text{H}_2\text{O}/\text{Ar}$  for oxidation were alternately poured for 1 h. Ar was purged between each reduction and oxidation step for 1 h.

The oxygen transfer properties of the  $\text{NiFe}_2\text{O}_4/\text{GDC}$  composite oxygen carrier materials based on the re-dox reaction were evaluated by means of thermal gravimetric analysis (TGA; TGA-N1000, Shinko, Korea) at  $900\text{ }^\circ\text{C}$ . 5%  $\text{H}_2/\text{Ar}$  and air were used as the reducing and oxidizing gases, respectively. Between each reduction and oxidation step, the reactor was purged with Ar for 3 min to prevent mixing of the reducing and oxidizing gases.

## Results and Discussion

The XRD patterns of the  $\text{NiFe}_2\text{O}_4$  samples synthesized and reacted with various gases are shown in Fig. 2.  $\text{NiFe}_2\text{O}_4$  powder synthesized at  $1,200\text{ }^\circ\text{C}$  for 3 h in air was formed in a single phase of spinel without any detectable impurity, and the diffraction peaks matched well with those of  $\text{NiFe}_2\text{O}_4$  (JCPDS No. 00-010-0325). Since the product gases for  $\text{CH}_4$  are  $\text{H}_2\text{O}$  and  $\text{CO}_2$ , as described in Eq. (2), oxygen carrier materials are

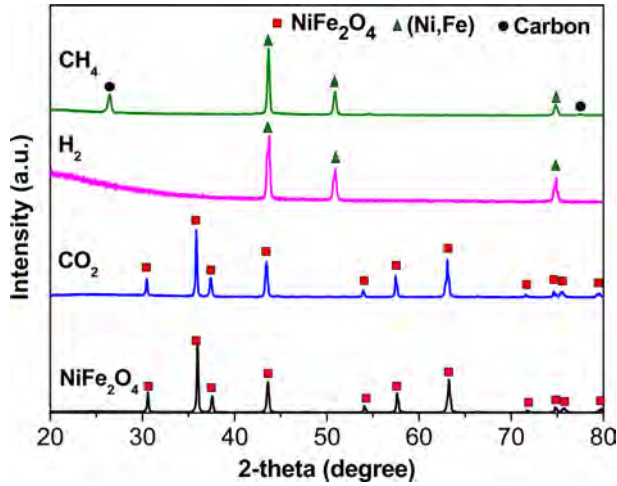


**Fig. 2.** XRD patterns of NiFe<sub>2</sub>O<sub>4</sub> obtained for the various reaction gases at 900 °C for 1 h.

exposed to a CO<sub>2</sub>-rich atmosphere in the fuel reactor. As shown in Fig. 2, no carbonate phases such as NiCO<sub>3</sub> or FeCO<sub>3</sub> were observed after the reaction with CO<sub>2</sub>. Therefore, NiFe<sub>2</sub>O<sub>4</sub> was not influenced by CO<sub>2</sub> in the fuel reactor at 900 °C. Meanwhile, the NiFe<sub>2</sub>O<sub>4</sub> powders reacted with H<sub>2</sub> and CH<sub>4</sub> at 900 °C for 1 h showed a single phase of (Ni,Fe) alloy. In the case of CH<sub>4</sub>, carbon peaks due to a methane cracking reaction (CH<sub>4</sub> → C + 2H<sub>2</sub>) were detected.

To confirm the re-dox mechanism of NiFe<sub>2</sub>O<sub>4</sub>, phase analysis was carried out after reduction in H<sub>2</sub> followed by oxidation in air or H<sub>2</sub>O. The (Ni,Fe) alloy, which was the NiFe<sub>2</sub>O<sub>4</sub> sample reduced in H<sub>2</sub>, did not return to NiFe<sub>2</sub>O<sub>4</sub> after re-oxidation in air, as shown in Fig. 3. If the (Ni,Fe) alloy was a stoichiometric compound such as NiFe<sub>2</sub>, the re-oxidized (Ni,Fe) alloy sample must have been a single phase of NiFe<sub>2</sub>O<sub>4</sub>. However, the sample re-oxidized in air showed two phases of NiFe<sub>2</sub>O<sub>4</sub> and Fe<sub>2</sub>O<sub>3</sub>. Therefore, the (Ni,Fe) alloy was formed in the Fe-rich composition such as Ni<sub>x</sub>Fe<sub>2</sub> (0 < x < 1). This can be confirmed by the XRF data, as shown in Table 1. It has also been reported that Ni can be volatilized in the presence of H<sub>2</sub>O at high temperatures [22].

The reduction of NiFe<sub>2</sub>O<sub>4</sub> took place as a stepwise process, and the following pathway is suggested: NiFe<sub>2</sub>O<sub>4</sub> → Ni-Fe<sub>2</sub>O<sub>3</sub> → Ni-Fe<sub>3</sub>O<sub>4</sub> → Ni-FeO → Ni-Fe [23]. Based on the composition and phase analysis, the reduction mechanism of NiFe<sub>2</sub>O<sub>4</sub> at 900 °C can be described as follows.

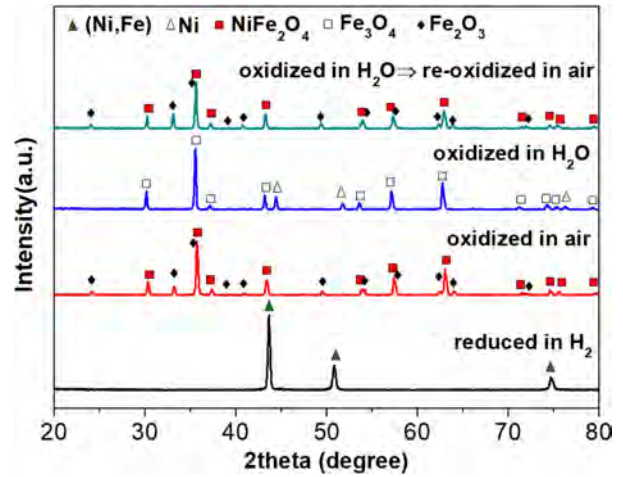
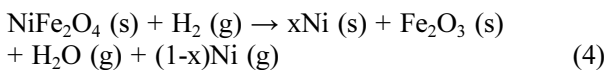
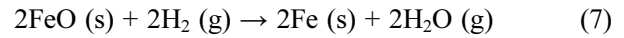
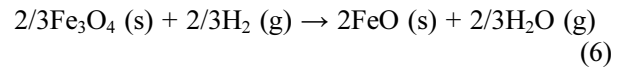
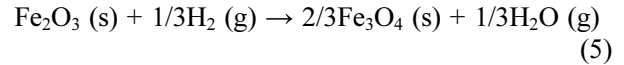
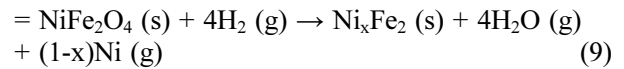
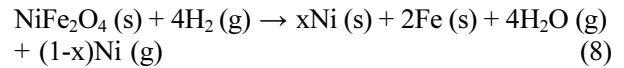


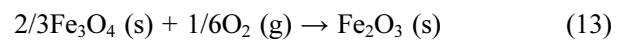
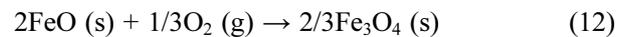
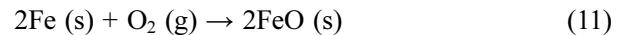
**Fig. 3.** XRD patterns of NiFe<sub>2</sub>O<sub>4</sub> according to re-dox reaction at 900 °C for 1 h.



Therefore, the overall reduction reaction in H<sub>2</sub> is as follows.



When Ni<sub>x</sub>Fe<sub>2</sub> was oxidized in air, the products were NiFe<sub>2</sub>O<sub>4</sub> and Fe<sub>2</sub>O<sub>3</sub> as shown in Fig. 3. Therefore, the reduced NiFe<sub>2</sub>O<sub>4</sub> (Ni<sub>x</sub>Fe<sub>2</sub>) reacted with oxygen in the air to induce the oxidation reaction as follows.



The overall oxidation reaction in air is as follows.

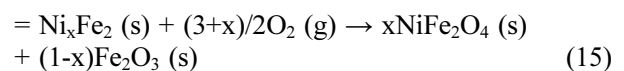
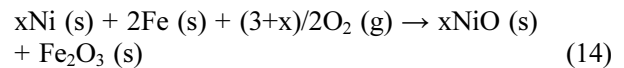
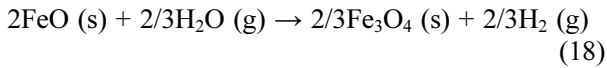


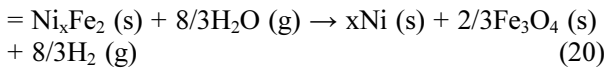
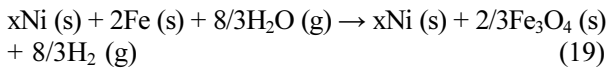
**Table 1.** XRF data for the NiFe<sub>2</sub>O<sub>4</sub> powder reduced by H<sub>2</sub> at 900 °C for 1 h.

Component	Fe	Ni	Al	K	Si	Cr	Mn	P	S
Amount (mass%)	65.838	33.711	0.162	0.115	0.101	0.036	0.024	0.007	0.006

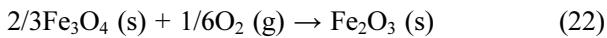
Meanwhile, it has been reported that reduced nickel oxide or metallic nickel are difficult to oxidize by steam due to thermodynamic limitations [14,19,23,24]. Therefore, most of the reduced nickel ferrite can only be oxidized to be a mixture of  $\text{Fe}_3\text{O}_4$  and Ni under steam. This result corresponds to the existence of  $\text{Fe}_3\text{O}_4$  and Ni phases in our sample oxidized in  $\text{H}_2\text{O}$ , as shown in Fig. 3. In the steam reactor,  $\text{Ni}_x\text{Fe}_2$  reacted with  $\text{H}_2\text{O}$  to induce the oxidation reaction as follows.



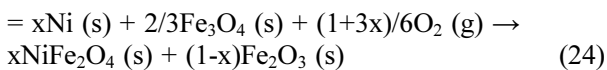
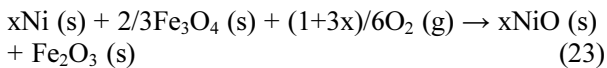
The overall oxidation reaction in steam is as follows.



When the oxygen carrier material oxidized in the steam reactor flowed into the air reactor, un-reacted Ni and  $\text{Fe}_3\text{O}_4$  became fully re-oxidized by oxygen as follows.



The overall re-oxidation reaction in air after the oxidation in steam is as follows.



XPS analysis was also performed in order to verify the valence state of Fe in  $\text{NiFe}_2\text{O}_4$  before and after the oxidation reaction at  $900^\circ\text{C}$  for 1 h. The XPS spectra obtained for the various atmospheres are shown in Fig. 4. The binding energies of Fe 2p<sub>3/2</sub>, Fe 2p<sub>3/2</sub> satellite, and Fe 2p<sub>1/2</sub> in  $\text{Fe}_2\text{O}_3$  are 711.0, 718.8, and 724.6 eV, respectively [25]. The peak positions of Fe 2p<sub>3/2</sub>, Fe 2p<sub>3/2</sub> satellite, and Fe 2p<sub>1/2</sub> in  $\text{NiFe}_2\text{O}_4$  in this study were observed at 711.0, 719.1, and 724.3 eV, respectively, which indicates that the valence state of Fe in  $\text{NiFe}_2\text{O}_4$  is 3<sup>+</sup>. Moreover, Dey et al. reported that the deconvolution of the Fe 2p peak of the  $\text{NiFe}_2\text{O}_4$  into two components correspond to the octahedral 2p<sub>3/2</sub> and 2p<sub>1/2</sub> peaks, and the tetrahedral 2p<sub>3/2</sub> and 2p<sub>1/2</sub> peaks [26]. The results are consistent with this study and indicate the absence of  $\text{Fe}^{2+}$  component and confirmation of the oxygen stoichiometric compound.

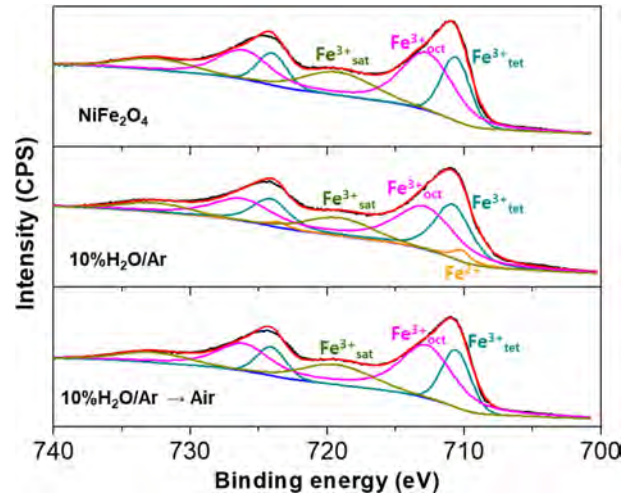


**Fig. 4.** XPS spectra of  $\text{NiFe}_2\text{O}_4$  before and after the oxidation reaction at  $900^\circ\text{C}$  for 1 h.

Alternatively, in the case of the sample oxidized in 10%  $\text{H}_2\text{O}/\text{Ar}$ , the peaks of  $\text{Fe}^{2+}$  (Fe 2p<sub>3/2</sub>) and  $\text{Fe}^{2+}$  (Fe 2p<sub>1/2</sub>) were identified at 710.2 and 723.7 eV, respectively. These results correspond to the peak positions of  $\text{Fe}_3\text{O}_4$  [25], indicating that the valence state of Fe in the sample oxidized in 10%  $\text{H}_2\text{O}/\text{Ar}$  is a mix of 2<sup>+</sup> and 3<sup>+</sup>. Interestingly, the peak positions of Fe 2p<sub>3/2</sub>, Fe 2p<sub>3/2</sub> satellite, and Fe 2p<sub>1/2</sub> in the sample re-oxidized in air are identical to those of  $\text{Fe}_2\text{O}_3$  and  $\text{NiFe}_2\text{O}_4$ .

The reduction and oxidation properties of  $\text{NiFe}_2\text{O}_4/\text{GDC}$  composite oxygen carrier materials were determined by  $\text{H}_2$ -TPR and  $\text{H}_2\text{O}$ -TPO, as shown in Fig. 5. It has been reported that  $\text{Fe}_2\text{O}_3$  exhibits a three-step reduction mechanism, with one reduction peak at a lower temperature ( $360\text{--}415^\circ\text{C}$ ) corresponding to the reduction of  $\text{Fe}_2\text{O}_3 \rightarrow \text{Fe}_3\text{O}_4$ , and two broad reduction peaks at  $500\text{--}750^\circ\text{C}$  and  $800\text{--}900^\circ\text{C}$  corresponding to reduction steps of  $\text{Fe}_3\text{O}_4 \rightarrow \text{FeO}$  and  $\text{FeO} \rightarrow \text{metallic Fe}$ , respectively [27–29]. It has been also reported that the  $\text{H}_2$ -TPR pattern of bulk NiO consists of one broad peak in the range of  $327$  to  $677^\circ\text{C}$  with a maximum peak at  $409^\circ\text{C}$ . The results in the present study (Fig. 5a) were in good agreement with the previous works, which indicates that the established reduction mechanism is plausible. In particular, the peak corresponding to the reduction steps of  $\text{Fe}_3\text{O}_4 \rightarrow \text{FeO}$  shifted to the low-temperature region with increasing GDC content. Based on the  $\text{H}_2$ -TPR data, it can be concluded that the reduction reactivity of the  $\text{NiFe}_2\text{O}_4/\text{GDC}$  composite slightly increased with increasing the amount of GDC. Similarly, based on the  $\text{H}_2\text{O}$ -TPO data (Fig. 5b), it is expected that the amount of oxidation reaction as well as the oxidation reactivity of  $\text{NiFe}_2\text{O}_4/\text{GDC}$  composite will increase with increasing the GDC content.

The XRD patterns of  $\text{NiFe}_2\text{O}_4/\text{GDC}$  composites before and after  $\text{H}_2$ -TPR and  $\text{H}_2\text{O}$ -TPO tests are shown in Fig. 6. All the XRD peaks of the samples before  $\text{H}_2$ -

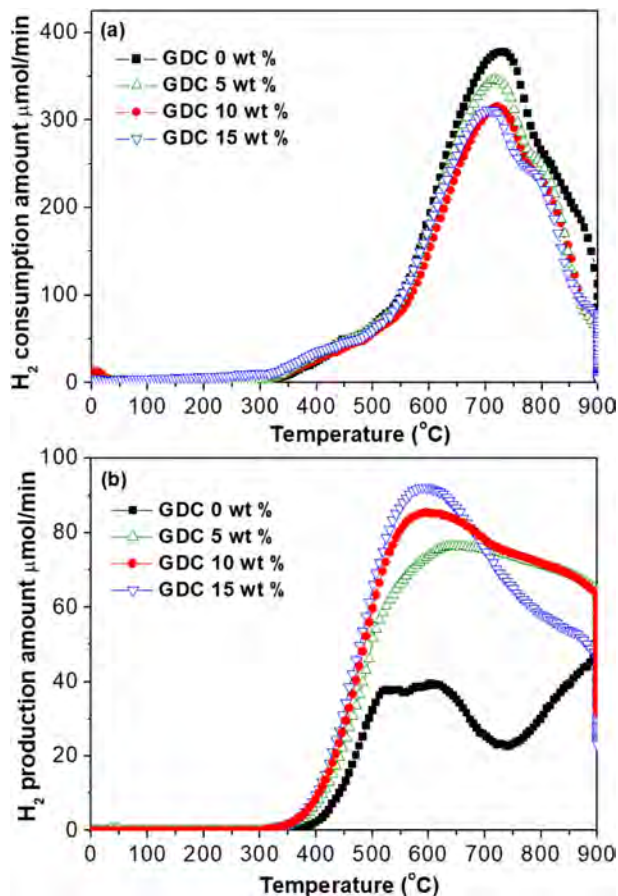


**Fig. 5.** (a) TPR data, and (b) TPO data of NiFe<sub>2</sub>O<sub>4</sub>/GDC composites obtained for 5% H<sub>2</sub>/Ar and 10% H<sub>2</sub>O/Ar as the reducing and oxidizing gases, respectively.

TPR and H<sub>2</sub>O-TPO tests (Fig. 6a) were matched with those of NiFe<sub>2</sub>O<sub>4</sub> or GDC, with no traces of secondary peaks. On the contrary, since the reduced NiFe<sub>2</sub>O<sub>4</sub> (Ni<sub>x</sub>Fe<sub>2</sub>) in the NiFe<sub>2</sub>O<sub>4</sub>/GDC composites during the H<sub>2</sub>-TPR test was oxidized to be a mixture of Ni and Fe<sub>3</sub>O<sub>4</sub> under steam during the H<sub>2</sub>O-TPO test, both Ni and Fe<sub>3</sub>O<sub>4</sub> peaks were detected after H<sub>2</sub>-TPR and H<sub>2</sub>O-TPO tests (Fig. 6b). Interestingly, CeFeO<sub>3</sub> was observed in the samples containing GDC. Mahmoodi et al. [30] also reported the formation of CeFeO<sub>3</sub> in the Fe<sub>2</sub>O<sub>3</sub>-CeO<sub>2</sub> oxygen carrier system during the re-dox cycle.

The microstructures of NiFe<sub>2</sub>O<sub>4</sub>/GDC composites before and after H<sub>2</sub>-TPR and H<sub>2</sub>O-TPO tests are shown in Figs. 7 and 8. All the samples had a porous structure before H<sub>2</sub>-TPR and H<sub>2</sub>O-TPO tests (Fig. 7a-d), and the fine GDC particles were evenly distributed over the NiFe<sub>2</sub>O<sub>4</sub> particles (Fig. 7b-d). Notably, the NiFe<sub>2</sub>O<sub>4</sub> sample without GDC exhibited severe agglomeration after the H<sub>2</sub>-TPR and H<sub>2</sub>O-TPO tests (Fig. 8a), while the well-dispersed GDC particles in the NiFe<sub>2</sub>O<sub>4</sub>/GDC composites (Fig. 8b-d) suppressed the aggregation of NiFe<sub>2</sub>O<sub>4</sub> particles and maintained the porous structure.

Fig. 9 shows the amount of H<sub>2</sub> consumption and production at 900 °C in the fuel reactor with 5% H<sub>2</sub>/Ar

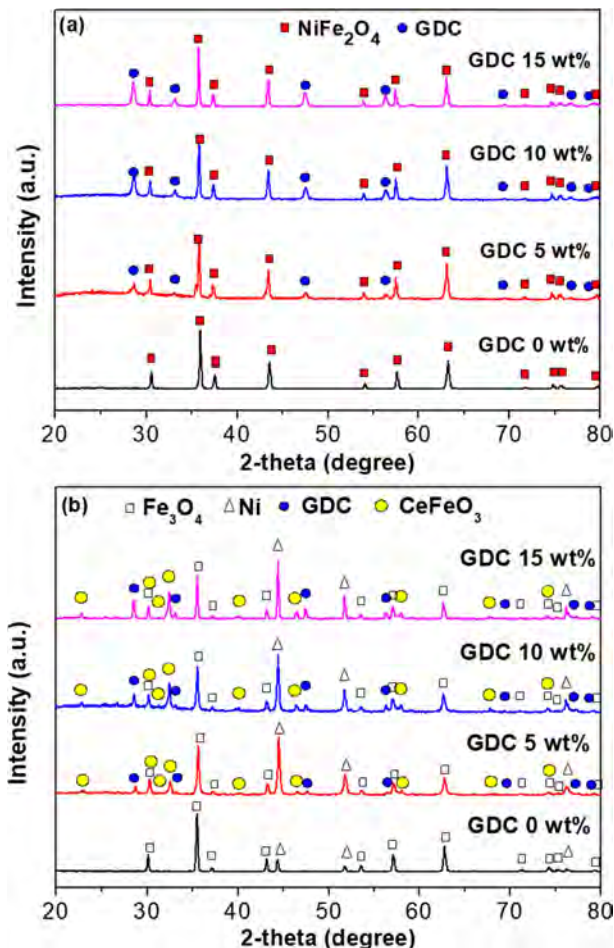


**Fig. 6.** XRD patterns of NiFe<sub>2</sub>O<sub>4</sub>/GDC composites (a) before and (b) after H<sub>2</sub>-TPR and H<sub>2</sub>O-TPO tests.

and in the steam reactor with 10% H<sub>2</sub>O/Ar, respectively. After the first cycle, the amount of H<sub>2</sub> consumption decreased significantly (Fig. 9a). This indicates that the reduced NiFe<sub>2</sub>O<sub>4</sub> (Ni<sub>x</sub>Fe<sub>2</sub>) could not be fully oxidized to NiFe<sub>2</sub>O<sub>4</sub> by H<sub>2</sub>O. This may be ascribed to the deactivation problem caused by the agglomeration of Ni. The oxidation-reduction reaction was limited to only a part of the agglomerated Ni surface after the first cycle. The amount of H<sub>2</sub> production in each cycle (Fig. 9b) was similar to that of H<sub>2</sub> consumption in the second and third cycles (Fig. 9a), while the amount of H<sub>2</sub> consumption and production of the NiFe<sub>2</sub>O<sub>4</sub>/GDC composites in the fuel and the steam reactor, respectively, increased with increasing GDC content. This might have been due to the suppression of agglomeration by the well-dispersed GDC particles, as shown in Fig. 8.

The maximum reaction rates of the NiFe<sub>2</sub>O<sub>4</sub>/GDC composites, as shown in Fig. 10, were also similar to the amount of H<sub>2</sub> consumption (Fig. 9a) and production (Fig. 9b) for the re-dox reaction. Because the re-dox reaction rate increased in proportion to the number of active sites where H<sub>2</sub> or H<sub>2</sub>O could react, the maximum reaction rates for the reduction (Fig. 10a) and oxidation (Fig. 10b) increased with increasing GDC content.

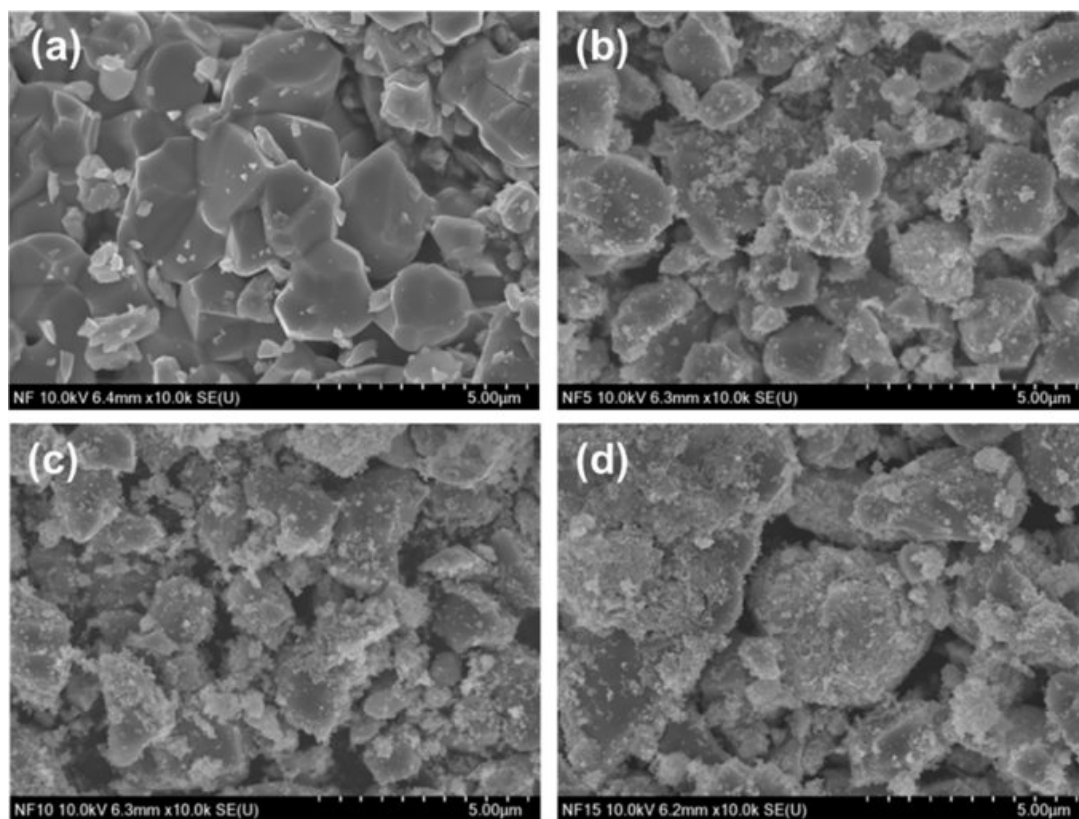


**Fig. 7.** FE-SEM images of  $\text{NiFe}_2\text{O}_4/\text{GDC}$  composites before  $\text{H}_2$ -TPR and  $\text{H}_2\text{O}$ -TPO tests: (a) 0 wt% GDC, (b) 5 wt% GDC, (c) 10 wt% GDC, and (d) 15 wt% GDC.

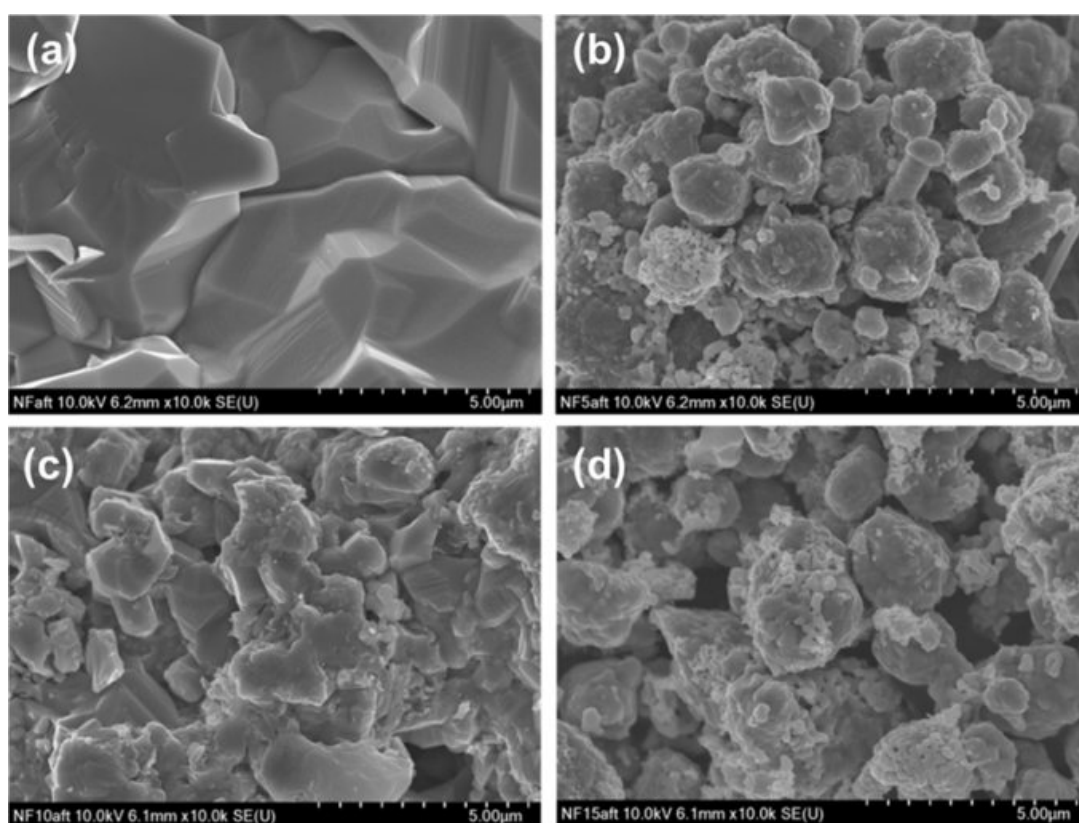


**Fig. 8.** FE-SEM images of  $\text{NiFe}_2\text{O}_4/\text{GDC}$  composites after  $\text{H}_2$ -TPR and  $\text{H}_2\text{O}$ -TPO tests: (a) 0 wt% GDC, (b) 5 wt% GDC, (c) 10 wt% GDC, and (d) 15 wt% GDC.

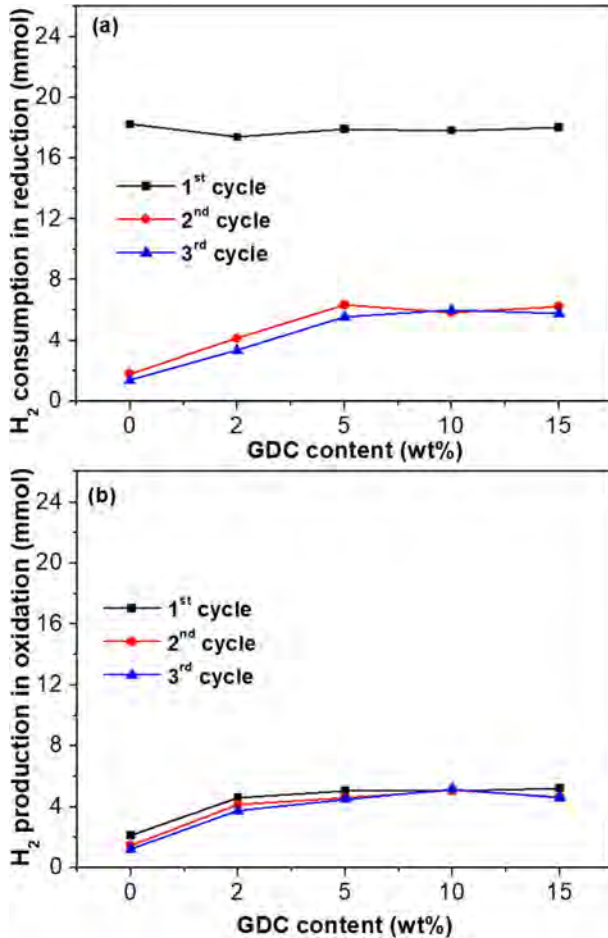


**Fig. 9.** (a) H<sub>2</sub> consumption, and (b) production of NiFe<sub>2</sub>O<sub>4</sub>/GDC composites versus GDC in reduction reaction with 5% H<sub>2</sub>/Ar and in oxidation reaction with 10% H<sub>2</sub>O/Ar, respectively, measured by GC.

We used TGA to evaluate the oxygen transfer properties of the NiFe<sub>2</sub>O<sub>4</sub>/GDC composite oxygen carrier materials based on the re-dox reaction between the fuel and air reactors. Re-dox curves of the NiFe<sub>2</sub>O<sub>4</sub>/GDC composites at 900 °C with 5% H<sub>2</sub>/Ar and air used as the reducing and oxidizing gases, respectively, are shown in Fig. 11. The empirical oxygen transfer capacity of NiFe<sub>2</sub>O<sub>4</sub> was 24.7 wt% at the first cycle, which was similar to the theoretical value of 27.3 wt% based on Eq. (9). However, in the case of NiFe<sub>2</sub>O<sub>4</sub> without GDC, the weight gain observed during oxidation was much smaller than the weight loss during reduction, indicating that the re-dox reaction was irreversible. This indicates that the oxygen transfer capacity of pure NiFe<sub>2</sub>O<sub>4</sub> degraded significantly during the re-dox cycle. In contrast, the NiFe<sub>2</sub>O<sub>4</sub>/15wt% GDC composite showed a full recovery of weight during oxidation.

The oxygen transfer rate ( $dX/dt$ ), referring to the change in the conversion rate per unit time, can be calculated from TGA data (Fig. 11). Fig. 12 shows the oxygen transfer rate of the NiFe<sub>2</sub>O<sub>4</sub>/GDC composite for reduction and oxidation reactions, respectively. The

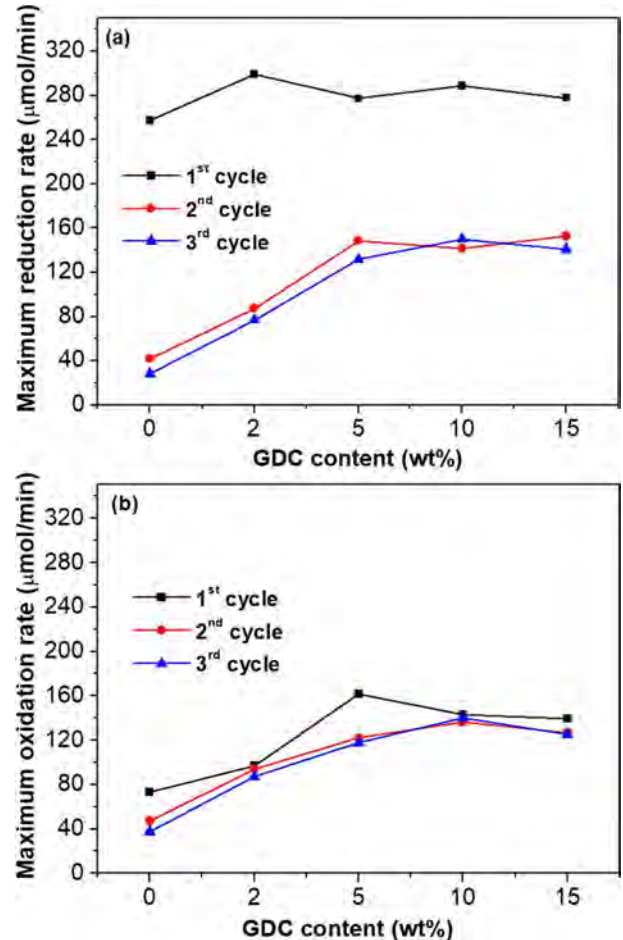


**Fig. 10.** Maximum reaction rate of NiFe<sub>2</sub>O<sub>4</sub>/GDC composites versus GDC content for (a) the reduction with 5% H<sub>2</sub>/Ar and (b) the oxidation with 10% H<sub>2</sub>O/Ar, measured by GC.

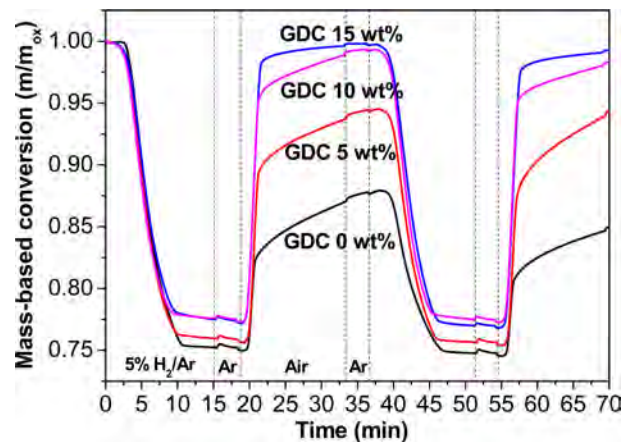


**Fig. 11.** Re-dox curves of the NiFe<sub>2</sub>O<sub>4</sub>/GDC composites at 900 °C with 5% H<sub>2</sub>/Ar and air used as the reducing and oxidizing gases, respectively, measured by TGA.

oxygen transfer rates for the reduction (Fig. 12a) and oxidation (Fig. 12b) reactions increased with increasing the GDC content. This suggests that GDC may affect the reaction kinetics of NiFe<sub>2</sub>O<sub>4</sub>/GDC composites.

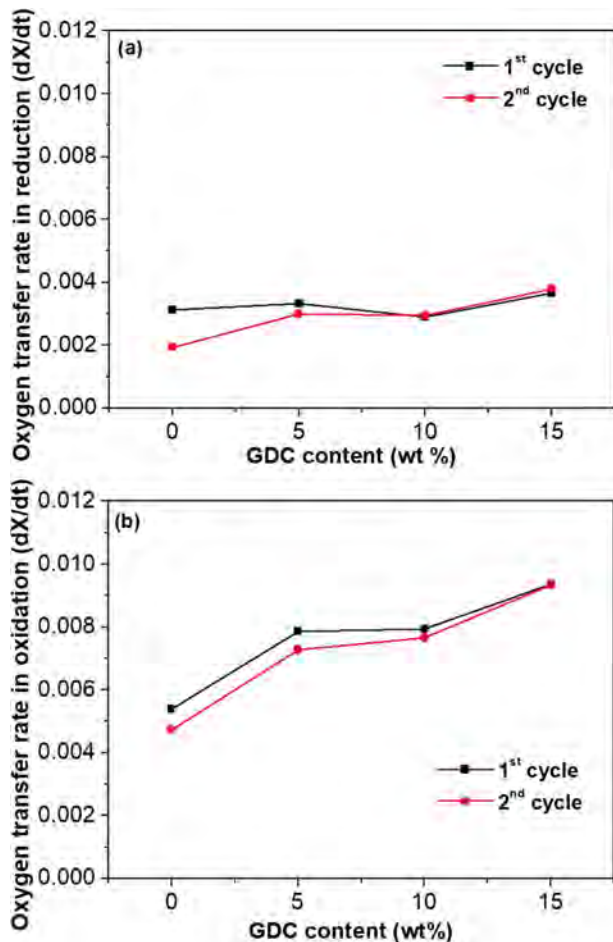


**Fig. 12.** Maximum oxygen transfer rate of  $\text{NiFe}_2\text{O}_4/\text{GDC}$  composites versus GDC content for (a) the reduction reaction with 5%  $\text{H}_2/\text{Ar}$  and (b) the oxidation reaction with air, measured by TGA.

Interestingly, the oxygen transfer rate for the oxidation reaction increased significantly for the composite that included 15 wt% GDC, as shown in Fig. 12(b).

It has been reported that GDC has oxygen storage capability due to its oxygen vacancies [31,32]. It is also well known that the surface adsorption of the reaction gas improves with the amount of oxygen vacancies on the surface. Therefore, the well-dispersed fine GDC particles on the surface of  $\text{NiFe}_2\text{O}_4$  can accelerate the surface adsorption of reaction gases due to the oxygen vacancies formed on the surface of the GDC. Moreover, fine GDC particles may suppress the grain growth of  $\text{NiFe}_2\text{O}_4$ . As a result, the specific surface area per unit volume of the  $\text{NiFe}_2\text{O}_4/\text{GDC}$  composite was larger than that of the pure  $\text{NiFe}_2\text{O}_4$ . This also increases the reaction rate in terms of the enlargement of active sites.

The primary advantage of the addition of GDC was that no significant agglomeration was observed before or after the re-dox cycle. Therefore, one can expect that an  $\text{NiFe}_2\text{O}_4/\text{GDC}$  composite may exhibit oxygen carrying stability during long-term cycles, based on the result of the reversible re-dox reaction and microstructural

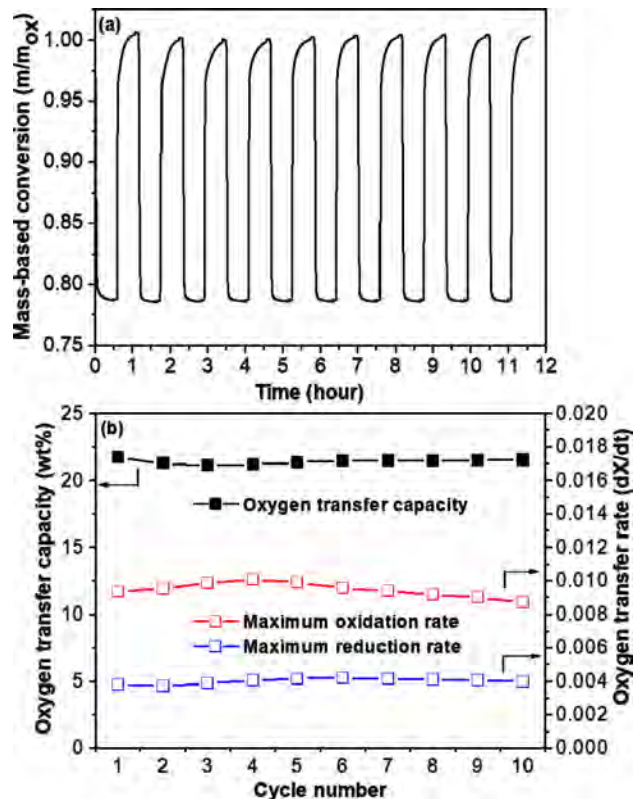


**Fig. 13.** (a) Re-dox curve, and (b) oxygen transfer capacity retention and rate stability of the  $\text{NiFe}_2\text{O}_4/15\text{wt}\% \text{GDC}$  composite at 900 °C during the 10 re-dox cycles, measured by TGA.

observation. Fig. 13(a) shows re-dox curve of the  $\text{NiFe}_2\text{O}_4/15\text{wt}\% \text{GDC}$  composite at 900 °C during the 10 re-dox cycles, measured by TGA. Based on the re-dox curve, the calculated oxygen transfer capacity retention and the variation of oxygen transfer rate are shown in Fig. 13(b). In fact, in this study the  $\text{NiFe}_2\text{O}_4/15 \text{wt}\% \text{GDC}$  composite showed no significant degradation in the oxygen transfer capacity and reaction rate after the tenth re-dox cycle, as shown in Fig. 13.

## Conclusions

This study characterizes  $\text{NiFe}_2\text{O}_4/\text{GDC}$  composites as oxygen carrier materials for CLHP. The re-dox mechanisms represented in the solid state in the fuel, in steam, and in the air reactor were  $\text{NiFe}_2\text{O}_4 \rightarrow \text{Ni}_x\text{Fe}_2$ ,  $\text{Ni}_x\text{Fe}_2 \rightarrow \text{Ni} + \text{Fe}_3\text{O}_4$ , and  $\text{Ni} + \text{Fe}_3\text{O}_4 \rightarrow \text{NiFe}_2\text{O}_4 + \text{Fe}_2\text{O}_3$ , respectively. Carbon dioxide could be captured from the fuel reactor and hydrogen could be produced from the steam reactor.

Both the amount and rate of hydrogen production for the  $\text{NiFe}_2\text{O}_4/\text{GDC}$  composites increased as the GDC content increased. Moreover, the oxygen transfer rate for both the reduction and oxidation reactions increased significantly with increasing GDC content. The positive effect of the addition of GDC may be mainly ascribed to an increase in the surface adsorption of reaction gases via the oxygen vacancies formed on the surface

of the GDC, as well as the enlargement of the active sites due to suppression of the agglomeration of  $\text{NiFe}_2\text{O}_4$  by the well-dispersed fine GDC particles on the surface of  $\text{NiFe}_2\text{O}_4$ .

In the case of the  $\text{NiFe}_2\text{O}_4/15\text{wt}\%$  GDC composite, no significant degradation in the oxygen transfer capacity or reaction rate during the re-dox cycles was observed. Assuming that the reaction rate of hydrogen production per hour is maintained, the amount of hydrogen production for the  $\text{NiFe}_2\text{O}_4/15\text{wt}\%$  GDC composite would be 2,702 L/day per unit mass (kg). In this regard, an  $\text{NiFe}_2\text{O}_4/\text{GDC}$  composite can be a promising oxygen carrier material for CLHP due to its high performance and stability. However, since the cost of the GDC is still high, trade-offs in terms of performance improvement and cost as well as industrial scalability should be considered. Therefore, it is necessary to develop a technology that can maximize performance while minimizing the content of GDC such as use of nano-composite powder.

### Acknowledgements

This research was supported by Basic Science Research Program through the National Research Foundation of Korea (NRF) funded by the Ministry of Education (2017R1D1A1B03031541). This work was also supported by the Technology Development Program to Solve Climate Changes of the National Research Foundation (NRF) grant funded by the Korea government (Ministry of Science and ICT) (2017M1A2A2044930).

### References

1. K.S. Go, S.R. Son, S.D. Kim, K.S. Kang, and C.S. Park, *Int. J. Hydrogen Energy* 34[3] (2009) 1301-1309.
2. R.D. Solunke and G. Veser, *Ind. Eng. Chem. Res.* 49[21] (2010) 11037-11044.
3. S. Dunn, *Int. J. Hydrogen Energy* 27[3] (2002) 235-264.
4. M. Momirlan and T.N. Veziroglu, *Renew. Sust. Energ. Rev.* 6[1-2] (2002) 141-179.
5. IPCC, in 2014: Climate Change 2014: Synthesis Report, 2015, edited by Pachauri, R. K., Allen, M. R., Barros, V. R., Broome, J., Cramer, W., Christ, R., Church, J. A., Clarke, L., Dahe, Q., Dasgupta, P., Dubash, N. K., Edenhofer, O., Elgizouli, I., Field, C. B., Forster, P., Friedlingstein, P., Fuglestvedt, J., Gomez-Echeverri, L., Hallegatte, S., Hegerl, G., Howden, M., Jiang, K., Jimenez Cisneroz, B., Kattsov, V., Lee, H., Mach, K. J., Marotzke, J., Mastrandrea, M. D., Meyer, L., Minx, J., Mulugetta, Y., O'Brien, K., Oppenheimer, M., Pereira, J. J., Pichs-Madruga, R., Plattner, G.-K., Pörtner, Hans-Otto, Power, S. B., Preston, B., Ravindranath, N. H., Reisinger, A., Riahi, K., Rusticucci, M., Scholes, R., Seyboth, K., Sokona, Y., Stavins, R., Stocker, T. F., Tschakert, P., van Vuuren, D. and van Ypserle, J.-P., Intergovernmental Panel on Climate Change Press (2015) p.151.
6. S.A. Rackley, in "Carbon Capture and Storage 2nd Edition" (Butterworth-Heinemann Press, 2017) p.22.
7. D.Y.C. Leung, G. Caramanna, and M.M. Maroto-Valer, *Renew. Sust. Energ. Rev.* 39 (2014) 426-443.
8. J. Gibbins and H. Chalmers, *Energy Policy* 36[12] (2008) 4317-4322.
9. V.J. Aston, B.W. Evanko, and A.W. Weimer, *Int. J. Hydrogen Energy* 38[22] (2013) 9085-9096.
10. P. Gupta, L.G. Velazquez-Vargas, and L.S. Fan, *Energy Fuels* 21[5] (2007) 2900-2908.
11. L.F. de Diego, M. Ortiz, F. García-Labiano, J. Adánez, A. Abad, and P. Gayán, *J. Power Sources* 192[1] (2009) 27-34.
12. M. Luo, Y. Yi, S. Wang, Z. Wang, M. Du, J. Pan, and Q. Wang, *Renew. Sust. Energ. Rev.* 81 (2018) 3186-3214.
13. L. Protasova and F. Snijkers, *Fuel* 181 (2016) 75-93.
14. F. Li, H.R. Kim, D. Sridhar, F. Wang, L. Zeng, J. Chen, and L.-S. Fan, *Energy Fuels* 23[8] (2009) 4182-4189.
15. Z. Huang, F. He, Y. Feng, K. Zhao, A. Zheng, S. Chang, G. Wei, Z. Zhao, and H. Li, *Energy Fuels* 28[1] (2014) 183-191.
16. M. Rydén and M. Arjmand, *Int. J. Hydrogen Energy* 37[6] (2012) 4843-4854.
17. J.R. Scheffé, M.D. Allendorf, E.N. Coker, B.W. Jacobs, A.H. McDaniel, and A.W. Weimer, *Chem. Mater.* 23[8] (2011) 2030-2038.
18. S. Yang, K. Kim, J.I. Baek, J.W. Kim, J.B. Lee, C.K. Ryu, and G. Lee, *Energy Fuels* 26[7] (2012) 4617-4622.
19. Y.L. Kuo, W.M. Hsu, P.C. Chiu, Y.H. Tseng, and Y. Ku, *Ceram. Int.* 39[5] (2013) 5459-5465.
20. Y.M. Choi, H. Abernathy, H.-T. Chen, M.C. Lin, and M. Liu, *Chem. Phys. Chem.* 7 (2006) 1957-1963.
21. C. Sun, H. Li, and L. Chen, *Energy Environ. Sci.* 5 (2012) 8475-8505.
22. G. Chen, G. Guan, Y. Kasai, and A. Abudula, *Int. J. Hydro. Energy* 37 (2012) 477-483.
23. S. Liu, F. He, Z. Huang, A. Zheng, Y. Feng, Y. Shen, H. Li, H. Wu, and P. Glarborg, *Energy Fuels* 30 (2016) 4251-4262.
24. K. Svoboda, A. Siewiorek, D. Baxter, J. Rogut, M. Puncochar, *Chem. Pap.* 61(2) (2007) 110-120.
25. T. Yamashita and P. Hayes, *Appl. Surf. Sci.* 254 (2008) 2441-2449.
26. J.K. Dey, A. Chatterjee, S. Majumdar, A.-C. Dippel, O. Gutowski, M.V. Zimmermann, and S. Giri, *Phys. Rev. B* 99 (2019) 144412.
27. T.S.T. Saharuddin, F. Salleh, A. Samsuri, R. Othaman, and M.A. Yarmo, *Int. J. Chem. Eng. Appl.* 6 (2015) 405-409.
28. G. Neri, A.M. Visco, S. Galvagno, A. Donato, and M. Panzalorto, *Thermochim. Acta* 329 (1999) 39-46.
29. X. Zhu, H. Wang, Y. Wei, K. Li, and X. Cheng, *J. Rare Earths* 28 (2010) 907-913.
30. F. Mahmoodi, S.H. Najibi, and A. Shariati, *J. Am. Sci.* 8[11] (2012) 453-459.
31. Y.M. Choi, H. Abernathy, H.-T. Chen, M.C. Lin, and M. Liu, *Chem. Phys. Chem.* 7 (2006) 1957-1963.
32. Z. Gu, K. Li, S. Qing, X. Zhu, Y. Wei, Y. Li, and H. Wang, *RSC Adv.* 4 (2014) 47191-47199.